Progress In Electromagnetics Research, PIER 72, 325–337, 2007

RADAR CROSS-SECTION STUDIES OF SPHERICAL LENS REFLECTORS

S. S. Vinogradov

CSIRO ICT Centre
PO Box 76, Epping, NSW, 1710, Australia

P. D. Smith

Department of Mathematics
Division of ICS, Macquarie University
NSW 2109, Australia

J. S. Kot and N. Nikolic

CSIRO ICT Centre
PO Box 76, Epping, NSW, 1710, Australia

Abstract—The reflectivity of a Spherical Lens Reflector is investigated. The scattering of an electromagnetic plane wave by a Spherical Lens Reflector is treated as a classical boundary value problem for Maxwell's equations. No restrictions are imposed on the electrical size of reflectors and the angular size of the metallic spherical cap. The competitiveness of the Spherical Lens Reflector against the Luneberg Lens Reflector is demonstrated. It has been found that Spherical Lens Reflectors with relative dielectric constant in the range $3.4 \leq \varepsilon_r \leq 3.7$ possess better spectral performance than 3- or 5-layer Luneberg Lens Reflectors in a wide frequency range.

1. INTRODUCTION

The Spherical Lens (SL) is a homogeneous dielectric sphere [1] which, for all dielectric constants in the range $1 \leq \varepsilon_r \leq 4$, focuses paraxial rays to a point z_{GO} outside the sphere. The distance from the centre of the lens to z_{GO} is f, the paraxial focal length, which may be determined

by Geometrical Optics, and is given in normalized form by

$$\frac{f}{r_1} = \frac{\sqrt{\varepsilon_r}}{2 \cdot (\sqrt{\varepsilon_r} - 1)} \tag{1}$$

where r_1 is the radius of the SL.

At microwave frequencies the more popular choice for the design of efficient reflectors is a stepped-index Luneburg Lens (LL) with attached metallic spherical cap [2–6]. In this paper we consider the possibility of replacing the relatively-expensive-to-manufacture LL by the cheaper SL. The use of SLs for antenna design has been intensively discussed in the 50's and 60's (see, for example [7, 8]). Nowadays, this idea appears to be undergoing a modest revival [9, 10]. In this connection, accurate focal studies of SLs are very instructive for making the optimal choice of the spherical cap location. The formula (1) is only a gross estimate; indeed the very idea of a "focal distance" or a "focal point" is somewhat idealized. At microwave frequencies the lens produces a finite region of space containing a high intensity electromagnetic (EM) field, usually called the "focal region". The characteristic size of the focal region or "focal spot" is comparable with a wavelength. Some results on EM energy density distribution in spherical lenses can be found in [11] and [12]. In general, the focusing properties of a three-parameter class of oblate Luneberg-like inhomogeneous lenses are studied in [13].

Whatever the size of the focal spot, when it is overlapped by a properly designed spherical metallic capcap, as shown in Figure 1, it produces a powerful reflection. This simple idea lies at the core of the design of both Luneberg Lens Reflectors ($LLRs$) and Spherical Lens Reflectors ($SLRs$). From a qualitative point of view it is quite evident that the minimal size of a cap to be chosen is that which slightly exceeds the extent of the focal spot. The objective of this paper is to demonstrate the competitiveness of $SLRs$ against the $LLRs$. The calculation of the radar cross-section (RCS) for $SLRs$ employs previously constructed algorithms which are valid for stepped-index $LLRs$ [5, 6]. When a spherical cap is attached to the surface of a SL, no dielectric shells exist outside of the core and we use the limiting case of algorithms developed in [5, 6]. The rigorous approach, developed in [5] and [6], tackles the case of the normal incidence. Recently, we proposed a highly efficient numerical method which enables us to treat the discussed problem for any incidence angle [14].

When a spherical cap is located at a distance from the SL's surface we enforce a "two-layer" model with a virtual concentric air shell surrounding the core and extending from the SL's interface $r = r_1$ to $r = r_2$, where $r = r_2$ is the radial spherical polar co-ordinate describing

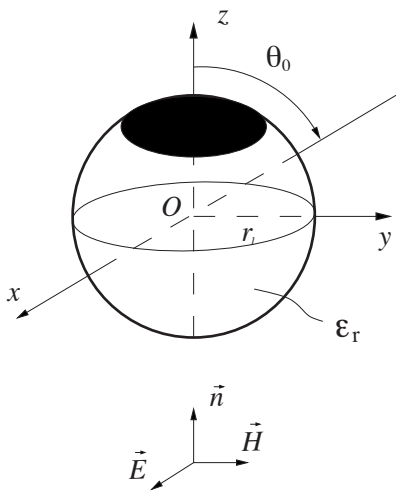

Figure 1. Electromagnetic plane wave incident on dielectric sphere with attached metallic spherical cap.

the cap's location ($r = r_2$, $0 \leq \theta \leq \theta_0$, $0 \leq \phi \leq 2\pi$).

The paper is organized as follows. In Section 2 we study the distribution of the *EM* field in the focal region of the dielectric spherical lens in an extremely wide-band frequency range, extending to deep optics ($k_0 r_1 = 15000$). Section 3 contains numerical results on the spectral dependence of *RCS* for reflectors based on *LL* and *SL*. It is demonstrated that *SLs* with a relative dielectric constant $\varepsilon_r = 3.5-3.7$ and attached metallic spherical cap produce better performance than or 3- or 5-layer *LLR*. In the Conclusion we discuss further studies of *SLRs* characterized by relative dielectric constants $\varepsilon_r > 4$ when the focal region of the *SLs* lies entirely inside the dielectric sphere.

2. FOCAL REGION OF A DIELECTRIC SPHERICAL LENS

The field distribution in the focal region of a dielectric spherical lens has been studied by many authors (see for example [11, 12]). Our studies are based on the classical Mie series solution for a homogeneous dielectric sphere. The numerical routine involves the calculation of spherical Bessel functions and associated Legendre functions. For the sake of space we do not describe the complete numerical details of the Mie series computations since this is a well-established procedure. The objective of these studies is to evaluate the characteristic size of a focal

spot depending on relative dielectric constant, ε_r and electrical size of a spherical lens, $2\,r_1/\lambda$. The realistic electrical size at microwaves for practical *SLRs* varies within the range $5 \leq 2r_1/\lambda \leq 200$, though our code enables us to advance into the extremely deep optical region where the parameter $2\,r_1/\lambda$ may take values up to 10000 ($k_0 r_1 \sim 30000$). The dielectric constant ε_r varies from 2.1 (PTFE) to 3.8 (fused quartz).

The dB-scaled distribution of the EM energy density W across the optical axis (the z-axis) for a SL with $\varepsilon_r = 2.1$ is shown in Figure 2 where the parameter $2\,r_1/\lambda$ takes the values 20, 50, 100 and 200 respectively. Similar results with $\varepsilon_r = 2.6$ are shown in Figure 3. The formula (1) in the case of the dielectric constant $\varepsilon_r = 2.1$ and $\varepsilon_r = 2.6$ estimates the GO focus to be placed at the points $z_{GO} = 1.613 \cdot r_1$ and $z_{GO} = 1.316 \cdot r_1$, respectively. In fact, for $\varepsilon_r = 2.1$, four local maxima of the EM energy density W occur at the points $z = 1.270 \cdot r_1$, $z = 1.375 \cdot r_1$, $z = 1.445 \cdot r_1$ and $z = 1.488 \cdot r_1$, as shown in Figure 2. For $\varepsilon_r = 2.6$ and the same values $2\,r_1/\lambda = 20$, 50, 100, and 200, the corresponding four local maxima occur at the points $z/r_1 = 1.100$, 1.170, 1.199, and 1.230. These values are still far away from the GO predictions, even for $2\,r_1/\lambda = 200$. Because of the huge spherical aberrations the very meaning of the "focal point" at higher frequencies becomes lost since the neighboring peaks of the EM energy density W form a train of local maxima, of nearly equal value. In this chain, the local maximum which nearly corresponds to the focusing of the paraxial rays, slightly prevails in value. As the electrical size $2\,r_1/\lambda$ increases slightly, the position of this maximum shifts closer to the GO focal point. For $2\,r_1/\lambda = 500$, 1000, 2000 and $\varepsilon_r = 2.6$ the maximum of the EM intensity is shifted to the points $z/r_1 = 1.259$, 1.277 and 1.287 while formula (1) predicts $z_{GO}/r_1 = 1.316$.

For dielectric constant $\varepsilon_r = 3.5$ the distribution $W(z/r_1)$ is shown in Figure 4 for $2\,r_1/\lambda = 20$, 50, 100, 200 and in Figure 5 for $2\,r_1/\lambda = 1000, 2000$.

When, $\varepsilon_r = 3.5$ the GO prediction (1) for relative focal distance is $z_{GO}/r_1 = 1.072$. As the electrical size of the SL increases through the values $2\,r_1/\lambda = 20$, 50, 100, 1000 and 2000, the real location of the maxima of EM energy density W shifts slowly to the GO prediction: $z/r_1 = 0.896$, 0.988, 0.999, 1.0498, 1.0570. It can be seen from Figure 4 that the plot of $W(z/r_1)$ for $2\,r_1/\lambda = 200$ exhibits quite different behavior featuring two maxima within a transitional region between the interior and exterior of the SL. The first maximum lies at the point, $z/r_1 = 0.960$, where $W = 40.92\,\mathrm{dB}$, and the second one at the point $z/r_1 = 1.022$ where $W = 40.75\,\mathrm{dB}$.

The energy density distribution along the z-axis as well as the amplitude-phase distribution of the EM field are of paramount

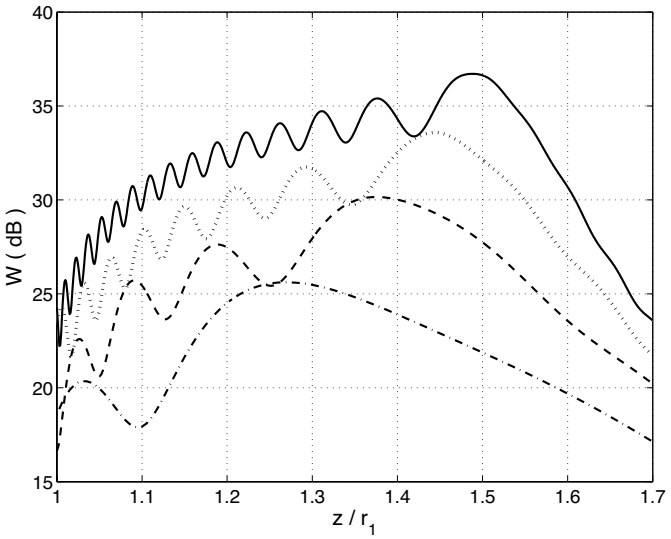

Figure 2. Distribution of the dB-scaled EM energy density across the optical axis of the SL ($\varepsilon_r = 2.1$): $2\,r_1/\lambda = 20$ (dot-dash), 50 (dashed), 100 (dotted), 200 (solid).

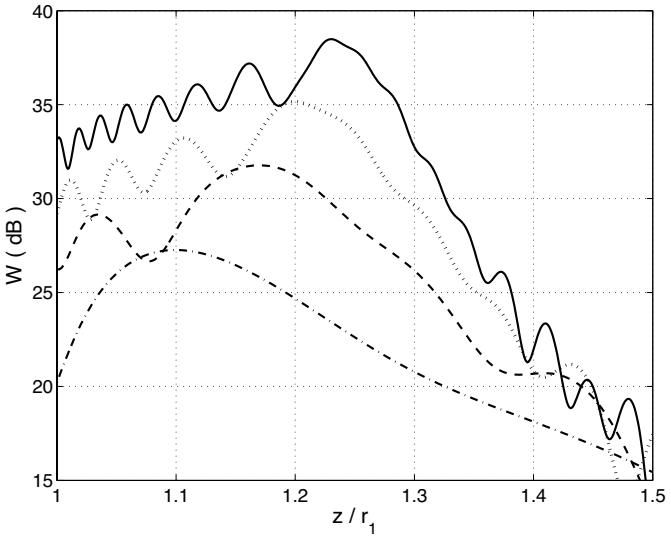

Figure 3. Distribution of the dB-scaled EM energy density across the optical axis of the SL ($\varepsilon_r = 2.6$): $2\,r_1/\lambda = 20$ (dot-dash), 50 (dashed), 100 (dotted), 200 (solid).

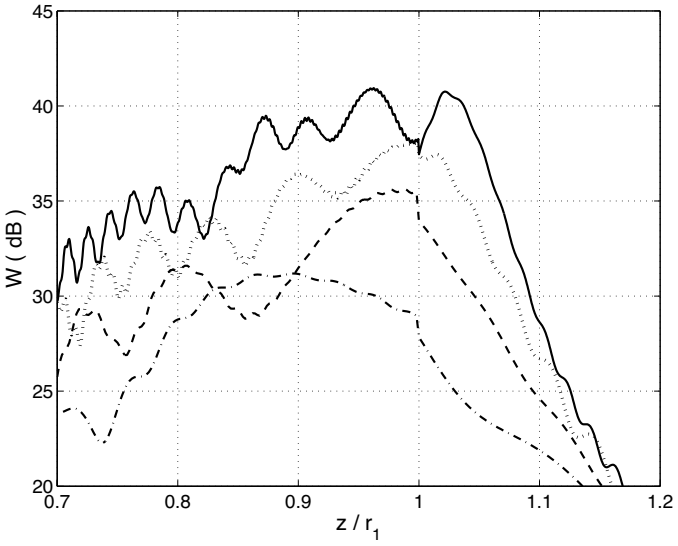

Figure 4. Distribution of the dB-scaled EM energy density across the optical axis of the SL ($\varepsilon_r = 3.5$): $2\,r_1/\lambda = 20$ (dot-dash), 50 (dashed), 100 (dotted), 200 (solid).

importance for antenna applications (see, for example, [15]) since this impacts the choice of the optimal position of a single feed and proper synthesis of a line feed. The optimal positioning of the feed relies on the partial suppression of the spherical aberrations. This improves the shape of radiation patterns by reducing the level of the first side-lobes, though always with some loss in the gain. In our case comprehensive studies of the amplitude-phase distribution of the EM field are not needed. What really matters is the size of the focused beam-width at the point of higher intensity EM field. With this in mind let us define the size of focal spot in a manner similar to definition of the half-power beamwidth ($HPBW$) in antenna theory, i.e., take the highest value among all local spots and to measure the distance from this point to that one where intensity drops by 3 dB. To estimate the size of this focal spot it is necessary to calculate the intensity distribution along the z-axis and after that, when the maximum of intensity is found (z_R/r_1), to fix this value and calculate the intensity distribution in the transversal plane. It is sufficient only to use two principal directions across the E-plane ($\phi = 0°$) and H-plane ($\phi = 90°$).

We implement this program for a SL with $\varepsilon_r = 3.7$ for $2\,r_1/\lambda = 10$, 20, 50, 100, 200. The corresponding values for the "focal point" are $z_R/r_1 = 0.778$, 0.855, 0.922, 0.962, 0.9995. The transverse size of the

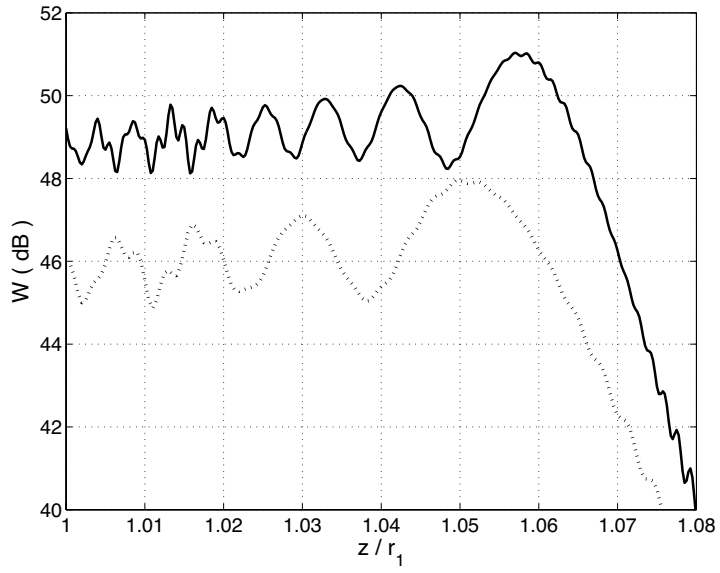

Figure 5. Distribution of the dB-scaled EM energy density across the optical axis of the SL ($\varepsilon_r = 3.5$): $2\,r_1/\lambda = 1000$ (dotted), 2000 (solid).

focal spot is evaluated from the distribution shown in Figure 6.

The focused beams are not rotationally symmetric. The difference in the $HPBW$ in E- and H-planes can be seen from the following table.

$2\,r_1/\lambda$	10	20	50	100	200
$(HPBW)_E/\lambda$	0.374	0.434	0.510	0.597	0.655
$(HPBW)_H/\lambda$	0.408	0.468	0.587	0.691	0.816

As the frequency (or electrical size $2\,r_1/\lambda$) increases the cross-section of the focused beam decreases spatially but the electrical size (in terms of the wavelength) increases. Based on these results one can deduce that, in order to reflect most energy at a fixed electrical size of the SL, it is sufficient to attach metallic spherical caps of angular sizes $2\theta_0 = 4.67°$, $2.68°$, $1.34°$, $0.79°$, $0.47°$ for $2\,r_1/\lambda = 10$, 20, 50, 100, 200, respectively, when $\varepsilon_r = 3.7$. Based on these results we can assert that interception of the beam energy within the range $10 \leq 2\,r_1/\lambda \leq 200$ can be realized when the minimal size of the spherical cap $2\theta_0 \approx 5°$. Similar results hold for ε_r varying from 2 to 4.

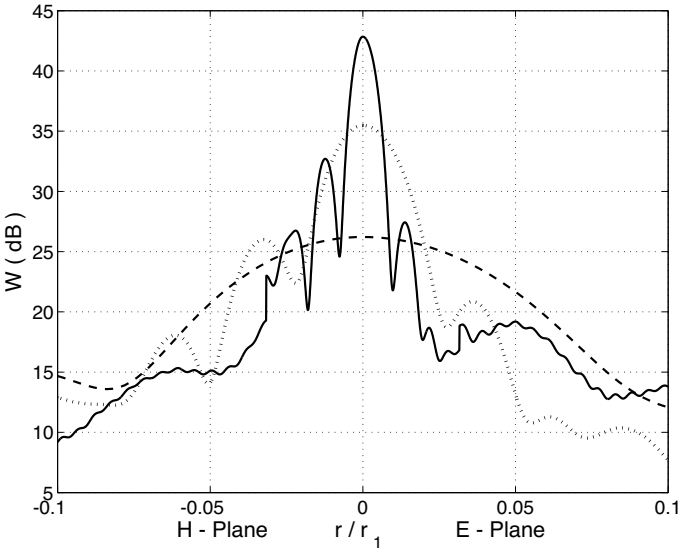

Figure 6. Shape of the focal spot in principal $E-$ and $H-$ plane for the SL ($\varepsilon_r = 3.7$) and $2\,r_1/\lambda = 10$ (dashed), 50 (dotted) and 200 (solid).

3. MONO-STATIC RCS OF THE *SLR* AT NORMAL INCIDENCE

All calculations of the RCS carried out in this Section are based on the results obtained in [5, 6] for the *Luneberg Lens Reflector (LLR)*. In [5] and [6] this problem is treated as a classical value problem for Maxwell's equations. The employment of the rigorous *Method of Regularization (MoR)* transforms the initial pair of coupled dual series equations into second kind infinite systems of the linear algebraic equations in two sets of Fourier coefficients. Any desired accuracy of computation is achievable depending on the size of the truncated systems. The constructed code is equally applicable to the studies of LLR and SLR. When a spherical cap is attached to the lens, the limiting case of this code is used where the lens incorporates only the core. When the spherical cap is separated at some distance from the lens interface we employ the two-layer model: core and virtual concentric air layer extending from the lens interface to spherical surface, part of which incorporates the cap. The standard definition of the mono-static RCS

is given by formula:

$$\sigma_B = \lim_{r\to\infty} 4\pi r^2 \frac{|E_\theta^{sc}|^2}{|E_\theta^{\circ}|^2} \tag{2}$$

where the scattered field intensity E_θ^{sc} is that observed in the direction which is opposite to the direction of the propagating EM plane wave. In most calculations we use the intrinsic normalization of the RCS dividing both parts of (2) by the physical cross-section of the lens, πr_1^2. This transforms (2) into a dimensionless quantity $\sigma_B^{(N)} = \sigma_B/\pi r_1^2$, which is useful for theoretical studies when the real geometrical size of the lens is unknown. As usual we calculate the dB-scaled value by the formula

$$(\sigma_B^{(N)})_{dB} = 10 \cdot \log_{10}(\sigma_B^{(N)}) \tag{3}$$

In the case of caps separated from the lens surface, we consider only such caps which are shadowed by the SL's. If r_c is the distance from the centre of the SL to the cap the permissible angular size of the cap θ_0 is defined by the formula:

$$\theta_0 \leq arcsin(\frac{r_1}{r_c}), r_c \geq r_1 \tag{4}$$

It was found in Section 2 that better candidates for the design of $SLRs$ with attached spherical cap are dielectric spheres (SLs) for which $\varepsilon_r = 3.5 - 3.7$ since they collect the rays close to the interface $r = r_1$ in a wide frequency band $10 \leq 2\,r_1/\lambda \leq 200$. The spectral dependences of the $SLRs$ with attached caps, $\theta_0 = 2.5^\circ$ and $\theta_0 = 60^\circ$, in the range $0.5 \leq 2\,r_1/\lambda \leq 200$ are shown in Figures 7 and 8 correspondingly.

It can be seen from these Figures that a larger cap provides a smoother dependence on $RCS(2\,r_1/\lambda)$. Furthermore, the overall performance of the SLR with $\varepsilon_r = 3.7$ is higher than one with $\varepsilon_r = 3.5$. Figure 9 demonstrates the competitiveness of the SLR against a reflector based on the uniform stepped-index LLR. We compare the spectral dependences $RCS(2\,r_1/\lambda)$ of the $SLR(\varepsilon_r = 3.7, \theta_0 = 60^\circ)$ and LLR with a realistic number of the layers $N = 3$ or 5. It can be seen from Figure 9, that the SLR performs better than a 3- or 5-layer LLR. When $N \geq 11$, the LLR features higher values of RCS against the SLR over the whole range $0.5 \leq 2\,r_1/\lambda \leq 200$. For consecutive values $N = 6$, 7, 8, 9, 10 the value for RCS for the LLR is higher than for the SLR in the range from $2\,r_1/\lambda = 0.5$ to $2\,r_1/\lambda = 35, 47, 58, 71, 90$ correspondingly. Up to $N = 10$ the dependence $RCS(2\,r_1/\lambda)$ has an oscillatory character. All this allows us to assert that the LLR can be effectively replaced by the much simpler SLR, which has a

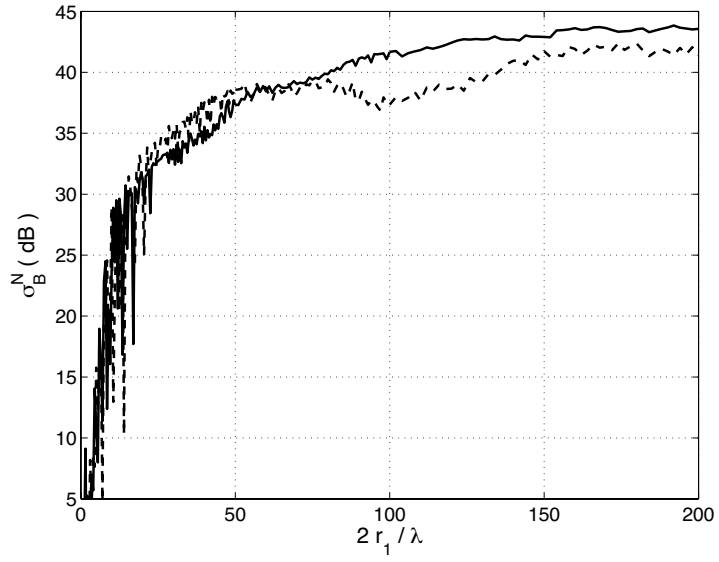

Figure 7. Normalized radar cross-section, σ_B^N, versus electrical size, $2\,r_1/\lambda$ of the SLR with $\theta_0 = 2.5°$, $\varepsilon_r = 3.5$ (dashed), 3.7 (solid).

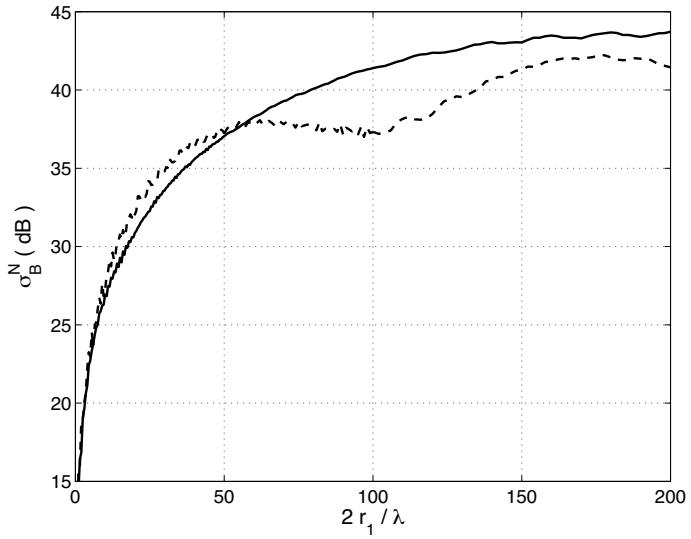

Figure 8. Normalized radar cross-section, σ_B^N, versus electrical size, $2\,r_1/\lambda$ of the SLR with $\theta_0 = 60°$, $\varepsilon_r = 3.5$ (dashed), 3.7 (solid).

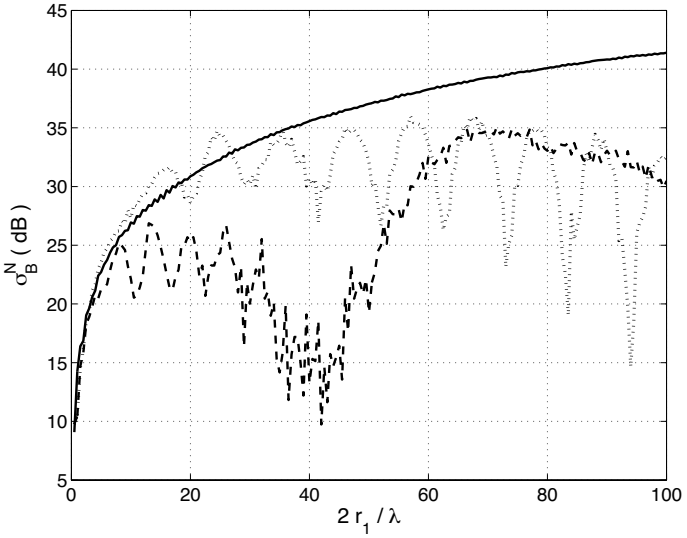

Figure 9. Comparative analysis of the spectral dependence for reflectors ($\theta_0 = 60°$) based on the SL ($\varepsilon_r = 3.7$) (solid), 3-layer (dashed) and 5-layer (dotted) LL.

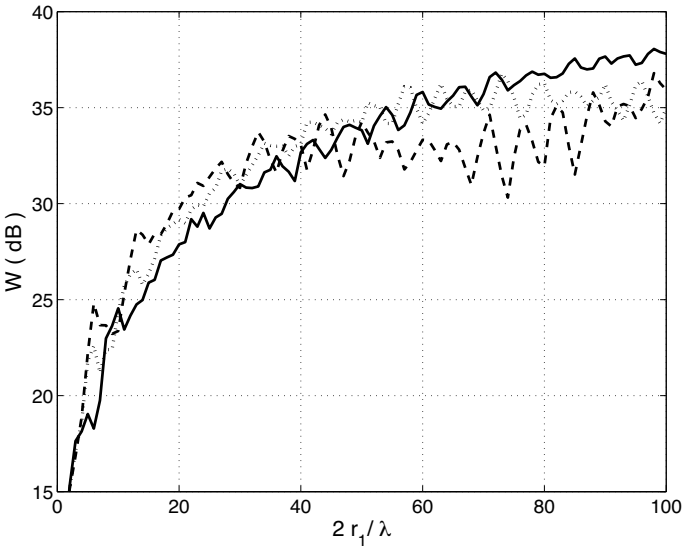

Figure 10. Reflectivity of the SLR with a distanced cap, $r_c/r_1 = 1.17$ (dashed), $r_c/r_1 = 1,199$ (dotted) and $r_c/r_1 = 1.23$ (solid).

high enough value RCS and a smooth, monotonic spectral dependence $RCS(2\,r_1/\lambda)$.

In the case of caps separated from the lens, they can be properly positioned to provide a high enough reflectivity but its level is less than for lenses with attached caps. Furthermore, the spectral dependence of radar cross-section for reflectors with caps separated from the lens is of oscillatory character. Figure 10 demonstrates such behavior. The dependence, $\sigma_B/\pi r_1^2$ versus electrical size, $2\,r_1/\lambda$ is plotted in Figure 10 for SLR with $\varepsilon_r = 2.6$ and separated cap of angular size $\theta_0 = 45°$. The spherical cap takes three positions along the optical axis, $r_c/r_1 = 1.17, 1.199, 1.23$ which correspond to the maxima of the EM field intensity for the SL at $2\,r_1/\lambda = 50, 100, 200$, respectively (see Section 2).

4. CONCLUSION

In this paper we have demonstrated the competitiveness of microwave reflectors based on simple spherical lenses against those based on stepped-index Luneburg lenses. After studies of the field distribution of the focused EM energy density, preference is given to the homogeneous dielectric spheres possessing dielectric constants in the range $\varepsilon_r = (3.5 - 3.7)$. These values of ε_r provide good focusing of a plane EM wave close to the spherical surface of the lens. When a metallic spherical cap is attached to the lens, this causes efficient reflection of the incident wave over a wide frequency range. The computation of RCS versus electrical size of the lens $2\,r_1/\lambda$ reveals the superiority of such a reflector over that based on the LL, in both value and smoothness of the spectral dependence RCS $(2\,r_1/\lambda)$. The focusing of the plane wave inside the lens is also of interest for microwave applications and we will consider further in our future work.

REFERENCES

1. Bekefi, G. and G. W. Farnell, "A homogeneous dielectric sphere as a microwave lens," *Can. J. Physics.*, Vol. 34, 790–803, 1956.
2. Sanford, J. R., "Analysis of spherical radar cross-section enhancers," *IEEE Trans. Antennas Propag.*, Vol. 43, No. 6, 1400–1403, 1995.
3. Sakurai, H., T. Hashidate, M. Ohki, K. Motojima, and S. Kozaki, "Electromagnetic scattering by the Luneberg Lens with reflecting cap," *IEEE Trans. Electromagn. Compat.*, Vol. 40, No. 2, 94–96, 1998.

4. Liang, C. S., D. A. Streater, J.-M. Jin, E. Dunn, and T. Rozendal, "A quantitative study of Luneberg-Lens Reflectors," *IEEE Antenna Propag. Mag.*, Vol. 47, No. 2, 30–41, 2005.
5. Smith, P. D. and S. S. Vinogradov, "A rigorous treatment of electromagnetic scattering by the Luneberg Lens Reflector," *Proc. of Int. Symposium on Electromagnetic Theory*, Vol. 1, 390–392, Thessaloniki, Greece, 1998.
6. Vinogradov, S. S., P. D. Smith, and E. D. Vinogradova, *Canonical Problems in Scattering and Potential Theory*, Part II: Acoustic and Electromagnetic Diffraction by Canonical Structures, Chapman & Hall/CRC, 2002.
7. Assaly, R. N., "Experimental investigation of a homogeneous dielectric sphere as a microwave lens," *Can. J. Phys.*, Vol. 36, 1430–1435, 1958.
8. Cheston, T. C., "Constant-K," *APL Tech. Dig.*, 8–11, 1963.
9. Schoenlinner, B., X. Wu, J. P. Ebling, G. V. Eleftheriades, and G. M. Rebeiz, "Wide-scan spherical-lens antennas for automotive radars," *IEEE Trans. on MTT*, Vol. 50, No. 9, 2166–2175, 2002.
10. Shavit, R., "Dielectric spherical lens antenna for wireless millimeter-wave communications," *Microwave and Optical Technology Letters*, Vol. 38, No. 1, 28–33, 2003.
11. Michel, F., G. Reidemeister, and S. Ohkubo, "Luneburg Lens approach to nuclear rainbow scattering," *Phys. Rev. Letters*, Vol. 89, No. 15, 152701-1-4, 2002.
12. Ji, Y. and K. Hongo, "Field in the focal region of a dielectric spherical lens," *J. Opt. Soc. Am. A*, Vol. 8, No. 11, 1721–1728, 1991.
13. Gizesik, J. A., "Focusing properties of a three-parameter class of oblate, Luneberg-like inhomogeneous lenses," *Journal of Electromagnetic Waves and Applications*, Vol. 19, No. 8, 1005–1019, 2005.
14. Nikolic, N., J. S. Kot, and S. Vinogradov, "Scattering by a Luneberg Lens partially covered by a metallic cap," *Journal of Electromagnetic Waves and Applications*, Vol. 21, No. 4, 549–563, 2007.
15. Boutayeb, A.-C. T. and K. Mahdjoubi, "Focusing characteristics of a metallic cylindrical electromagnetic band gap structure with defects," *Progress In Electromagnetics Research*, PIER 66, 89–103, 2006.